Defense Technical Information Center
Compilation Part Notice

ADP011821

TITLE: Study of Porous Silicon Formation and Silicon-on-Porous Silicon Epitaxy [Computational Modelling]

DISTRIBUTION: Approved for public release, distribution unlimited

This paper is part of the following report:

TITLE: NATO Advanced Research Workshop on Nanostructured Films and Coatings. Series 3. High Technology - Volume 78

To order the complete compilation report, use: ADA399041

The component part is provided here to allow users access to individually authored sections of proceedings, annals, symposia, etc. However, the component should be considered within the context of the overall compilation report and not as a stand-alone technical report.

The following component part numbers comprise the compilation report:
ADP011800 thru ADP011832

STUDY OF POROUS SILICON FORMATION AND SILICON-ON-POROUS SILICON EPITAXY (COMPUTATIONAL MODELLING)

P.L. Novikov, L.N. Aleksandrov, A.V.Dvurechenskii, V.A.Zinoviev

Institute of Semiconductor Physics, Academy of Science,

Novosibirsk 630090, Russia

E-mail: novikov@isp.nsc.ru

KEYWORDS/ ABSTRACT: porous silicon/ computer simulation/ fractal dimension/ epitaxy

By computer simulation the processes of porous silicon formation and of silicon-on-porous silicon epitaxy are studied. The model of electrochemical etching is applied for p^+Si and p^-Si substrates and takes into account the non-homogeneous surface charge distribution, the thermal generation of holes and quantum confinement effects. The epitaxy is studied on the basis of Gilmer model extended to the case of relief surface. The porous structures obtained by computer simulation are presented for various anodization conditions. The analysis of 3D images shows the profile of porosity over depth and multifractal properties. It is shown that the mechanism of epitaxy on PS (111) surface is provided by the thin pendant layer formation. The dependence of kinetics of epitaxy upon the porosity, molecular flow density and initial surface roughness are established.

1. Introduction

Porous silicon (PS), prepared by anodization, has become a very promising material for device application due to its visible luminescence [1], extremely large specific surface and wide technological opportunities [2, 3]. It is also an interesting subject for fundamental investigation, since fractal structure of PS exhibits a number of optical, transport and thermodynamic properties [4], which are not fully understood.

Along with experimental methods, the computer simulation has been used for the study of PS properties. The first step in this direction was the modelling of PS formation. The diffusion limited aggregation (DLA) model and its variations [5, 6]

256

appeared to be easily adapted for computer simulation. However, structures obtained in these computational experiments could hardly be used in further investigation mainly for the following reasons. First, these structures were modelled on the 2D meshes. Second, they had only visual resemblance to the real ones, while the detailed topological analysis showed that much of structural characteristics (such as shape and size distribution of pores, interface profiles etc.) were not quite adequate. The simulated porous structures obtained by Aleksandrov and Novikov [7] exhibited the variety of morphologies and the structural [8] and thermodynamic [9] properties of PS were studied. The qualitative analysis of the simulated PS layer surface was used for modelling of silicon-on-porous silicon epitaxy. The present paper includes the series of works which deal with the modelling of PS formation, structural analysis of various simulated morphologies and homoepitaxy on PS.

2. The model and method of calculation

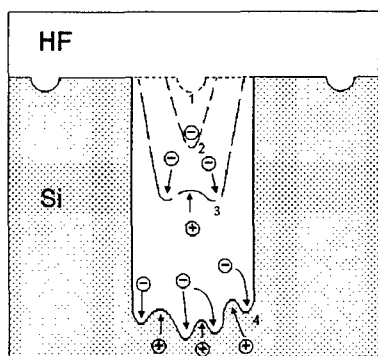### 2.1. THE MODEL OF POROUS SILICON FORMATION

Fig.1. Schematic illustration of the pore formation relief mechanism. The contours 1-4 show the consecutive stages of Si/HF interface evolution.

Since a hole is necessary in electrochemical reaction of Si dissolution under anodization, the actual question is at what points a hole preferably crosses the Si/HF interface. We suppose that the morphology of the porous structure is determined by self-consisting correlation between potential and geometrical relief at Si/HF interface. At the first stage of pore formation the initial flat and smooth silicon anode becomes a relief as the result of random dissolution (contour 1 in Fig.1). This stage proceeds until tips or cavities at the Si/HF interface become marked enough to trap the charge carriers (contour 2 in Fig.1). F⁻ ions are trapped in the cavities, filled with HF solution, while holes drift to the hillocks (contour 3 in Fig.1). If the electrolyte near the silicon anode is depleted (high current density approximation) then the hillocks are the effective centers for dissolution and electropolishing occurs. In the opposite case (low current density and/or light doping level and/or high HF concentration) electric field lines are focused on the pore tips, where the dissolution preferably takes place. In an intermediate case, when electrolyte is weakly depleted, only some randomly formed pores induce at their tips an electric field large enough to attract the holes effectively. The current density, j, at the tips of these pores is higher than the average over the surface and in the region of electrolyte near the pore tips the strong ion depletion is formed. This leads to the effect of "electropolishing" in micro regions near pore tips rather than over the whole surface. The size

of the micro regions determines an average diameter of pores, which is constrained by the condition of the depletion in the electrolyte at the pore tip. As the diameter of the

Fig.2. The illustration of the computational algorithm for p$^+$-PS formation.

pore exceeds some critical value D, the local current density (under the fixed average one) becomes too low to provide the strong depletion in the electrolyte. Then the region of "electropolishing" gets narrow. The pore diameter value is provided by the self-consistent processes.
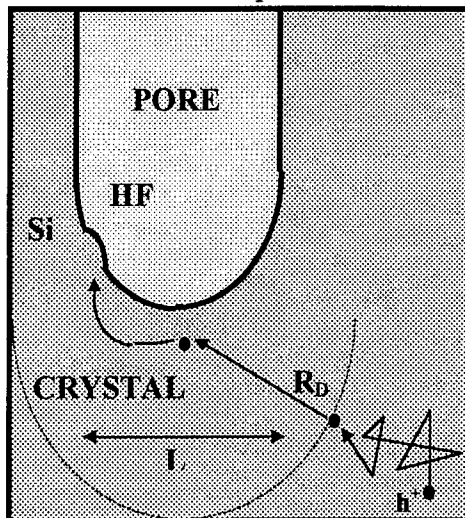
Computer simulation of p$^+$-Si anodization is performed on two-dimensional (160×160) mesh. Each position on the mesh is defined as a cell. One mesh step corresponds to the real size of surface charge fluctuations. The computational algorithm is illustrated in Fig.2. N holes undergo random transport by the mesh, hopping over a distance equal to the mean free path. As soon as a hole is located within radius R_D from the nearest pore tip, drift in the direction of this tip starts. R_D is equal to the Debye radius and expressed in mesh cells. After the hole reaches a point on the interface, the analysis of interface curvature is carried out within interval L from this point. The dissolution occurs in the most marked protuberance over the interval. The average diameter of pores, d, was estimated roughly as follows [7]:

$$d = \sqrt{\frac{4j}{Cc^{3/2}N_S}} \exp\left(\frac{E_A}{kT}\right) \qquad (1)$$

where c (wt.%) is HF concentration, N_S (cm^{-2}) is the surface density of pores, j (mA/cm^2) is anodic current density, T (K) is the temperature, E_A=343 meV, C=3300 mA·cm^{-2}·wt. %$^{-3/2}$. The parameter L (in mesh steps) is equal to d followed by Eq. (2).

In lightly doped crystal (p<10^{16} cm^{-3}) the space charge density and the local electrical field are low. Therefore, the effect of potential relief on the morphology of porous structure is expected to be negligible in this crystal. For this reason the dominant mechanisms of the pore formation are diffusion, thermal generation and recombination of holes and - in nanocrystallites - quantum confinement effect. The quantum confinement is known to increase the band gap. Consequently a barrier appears between the bulk region and nanoparticles, which prevents hole penetration inside nanoparticles. The size, at which the quantum confinement becomes significant, is denoted R_Q and equal to 10 nm and less [10].

Computer simulation of the pore formation in p$^-$-Si is performed on two-dimensional (160×160) and three-dimensional (160×160×80) meshes. One mesh step

corresponds to the average interatomic distance. The computational algorithm differs from the one described above. Hole may disappear from the current point and appear in another position of crystal volume with probability G. The generation rate g (s^{-1}) is linked to G by the relationship:

$$g=Gv_0/l, \tag{2}$$

where $l \sim 10^{-6}$-10^{-7} m is mean free path, $v_0 \sim 10^5$ m/s - mean velocity of hole. After a hole reaches the interface, the analysis of surrounding space is carried out. If the crystal volume contains the sphere of radius R_Q, then the dissolution occurs.

2.2. THE MODEL OF SILICON-ON-POROUS SILICON EPITAXY

The extended diffusion model was constructed on the basis of the initial premises of the Gilmer model and includes two new assumptions. First, vacancies and overhangs are permitted. Second, the summation of the second-nearest neighbors, which determine the activation energy of diffusion, extends over all 12 positions in the second coordination sphere. Evaporation of atoms is neglected. All numerical parameters of the extended model are corrected so that the growth process on the smooth Si (111) surface will occur identically to the process in the Gilmer diffusion model [11].

The computational algorithm is performed on a $N_X \times N_Y \times N_Z = 160 \times 160 \times 20$ three-dimensional grid whose nodes correspond to regular positions of atoms in the crystal structure of silicon. The state of the cells that are filled with atoms is characterized by the numbers N_1 and N_2 of neighbors in the first and second coordination spheres ($1 \leq N_1 \leq 4$, $1 \leq N_2 \leq 12$) respectively. Each atom executes a diffusion hop with probability p (N_1,N_2,T). The final position of a diffusion hop is chosen randomly among the unoccupied cells in the first and second coordination spheres. Transitions which result in an atom not having any neighbors in the first coordination sphere are forbidden (that is why $N_1 \neq 0$, $N_2 \neq 0$). The probability of a diffusion hop (with the condition that the endpoint position is free) equals

$$p(N_1,N_2,T)=p_0\exp(-E/kT), \; E=N_1 \cdot E_1+N_2 \cdot E_2, \tag{3}$$

where k is Boltzmann's constant, T is temperature, and $p_0=\exp((E_1+3E_2)/kT)$ is a factor chosen so that the probability of a diffusion hop on the free (111) surface equals 1. To decrease the amount of computation, a threshold probability p_S, which limits the number of "candidates" for a diffusion hop (active array) to atoms for which $p(N_1,N_2,T)>p_S$, is introduced. Scanning over the elements in an active array is performed during iteration. The time interval corresponding to one iteration is estimated as $\tau=\chi \cdot p_0/v$, where $v=2.5 \cdot 10^{13}$ s^{-1} is the frequency of atomic oscillations and $\chi=6/16$ is the coefficient that takes into account the ratio between the numbers of possible final positions for Is(111) in the Gilmer and the extended diffusion models.

The parameter E_2 characterizes the kinetics of attachment/detachment of atoms on the faces of the elementary layers. These processes were investigated by simulation method, and the value $E_2=0.2$ eV provided good agreement with experimental data [12]. Since in our model an adatom on a smooth surface has one neighbor in the first
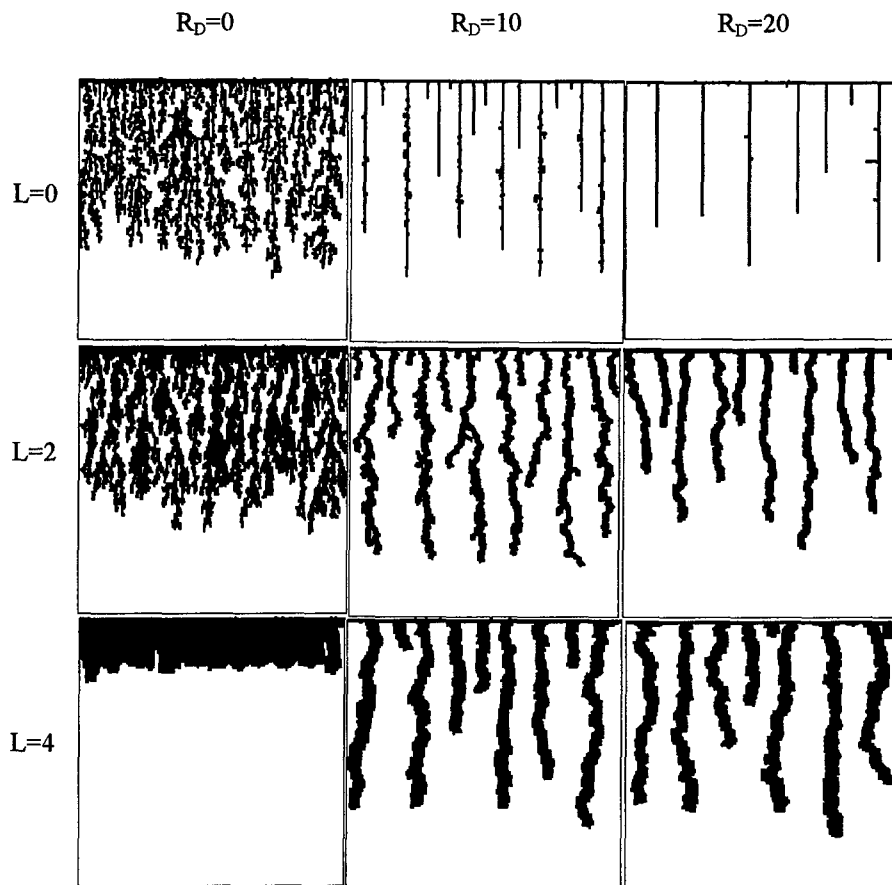
Fig. 3. A matrix of computer simulation plots with varying effective parameters L and R_D (N=80).

and three in the second coordination spheres, the activation energy of surface diffusion can be expressed as $E_A = E_1 + 3E_2$. At the same time, the value E_A=1.3±0.2 eV was obtained experimentally in a number of work. We employed the value E_A=1.34 eV, which corresponds to E_1=0.74 eV.

The probability that an atom from a molecular beam reaches the surface over time τ is

$$p_F = 2F\tau N_X N_Y, \qquad (4)$$

where F (bilayer/s) is the molecular flux density.

The 160×160×14 meshes speckled with bottomless cylindrical pores were used as the initial layer for simulation. The cylinders were randomly distributed over the surface and oriented normally to it. The number and radius of cylinders were the parameters of simulation.

3. Results and discussion.

3.1. RESULTS OF SIMULATION OF POROUS SILICON FORMATION.

A matrix of plots, obtained by computer simulation on two-dimensional mesh (160×160), with N=80 is shown at Fig.3. Black colour corresponds to pores. The pores grow downwards from the top of each plot. The effective parameters R_D and L (in mesh steps) are shown for each lin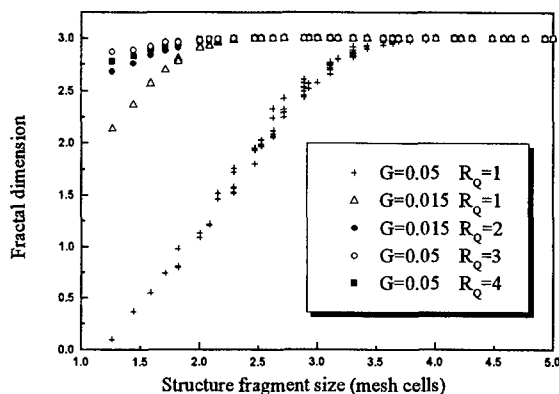e and column of the matrix. The pore diameter is seen to increase with the increase of L, which corresponds to current density increase and/or HF concentration decrease. This result agrees with experimental data [13, 14]. Within radius, L, pores are continuos in plane-parallel directions, which agrees with high-resolution and cross-sectional TEM photographs of the mesoporous Si layers [15]. For $L=4$ and $R_D=0$ current density is great enough to achieve polishing. R_D increase leads to straightening of the pores and increasing distance between them. By the conditions $L=0$ and $R_D=10$ and 20, the direction of growth is practically prede-termined, since the active zone for each pore is limited by its lowest point. Similar conditions were provided by Lehmann et. al. [16] in n-Si, using inducing pits and backside illumination.

Fig. 4. Fractal dimension of structures formed by computer simulation on three-dimensional mesh *vs* size of detail.

The three-dimensional images of simulated structures ($160 \times 160 \times 80$) were ob-tained. The calculations show that the porosity P changes over the depth, h, of the porous layer in accordance with SIMS data [17]. dP/dh decreases with increasing G. In order to interpret this result, it is necessary to first explain why the gradient in DLA model rises without hole generation ($G=0$). In the growth process limited by diffusion, holes can not penetrate from the bottom to the top of the growth layer since they are effectively captured by the branches of the ramified structure. For this reason the growth preferably proceeds in thin front layer. Let us characterize it at any time by the current active surface defined as the number of possible centres of growth in the front layer. The initial flat Si/HF interface has the highest active surface. As the cluster develops, the active surface decreases (even though the whole specific surface may increase). The evolution of the active surface determines the porosity profile, so the change in active surface leads to the porosity gradient. The hole generation permits

holes to appear at any depth of PS layer, and the active surface is no longer limited by the front layer. Then the pore diameter increases until the quantum confinement in crystal nanoparticles becomes essential. So the simultaneous action of hole generation and quantum confinement leads t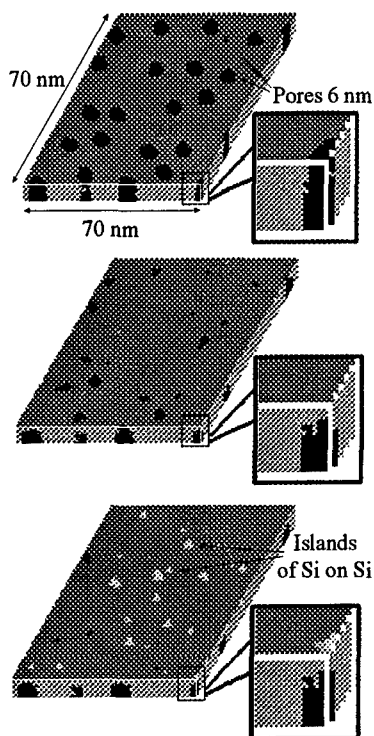o smoothing of the porosity profile. It was shown that a porosity averaged over the porous layer depth increases while R_Q decreases. This result is reasonable since the quantum confinement effect tends to prevent dissolution on the local scale.

The fractal dimension was calculated for the crystal part of the porous structures, formed by computer simulation on three-dimensional mesh. The dependence of fractal dimension upon size is shown in Fig.4. It changes from 0.1 to 3 as the size of the structure varies from 1.3 to 4 mesh steps, which corresponds to real sizes from 0.3 to 1 nm. The X-ray scattering experiment [18] showed that mesoporous structures are characterized by fractal dimension at sizes up to 100 nm. Nanoporous structures should display the fractal properties at smaller sizes.

3.2. THE RESULTS OF SIMULATION OF SILICON-ON-POROUS SILICON EPITAXY.

Three-dimensional images of grown layers were obtained for various porosity, pore size and molecular beam density, F. The typical fragments of layer surface before, during and after Si deposition on PS are shown in Fig. 5 (F=1 bilayer/s) and Fig. 6 (F=10 bilayer/s). The cross sections at the edges with the insets illustrate the pore morphology evolution. The difference in the kinetics of epitaxy for the cases of various F is clearly seen. Under low flow density, pores are the effective traps for adatoms and the Si island formation is suppressed until pores are covered. At high flow density, the adatoms form the islands between the pores. The islands are formed as far from the pores as a diffusion length. This is marked in case of large distance between the pores. Thus, the porosity chosen for Fig. 1 and Fig. 2 is rather low. It is an interesting result to find that a change in pore structure occurs only in the upper (of 1-2 bilayer thick) layer.

In order to specify the detailed mechanism of the Si growth over pores, the statistical analysis of random atomic bond configurations for adatoms inside pores was carried out. Figs. 6 a,b,c illustrate the idealized scheme for formation of Si pendant layer. Circles show the regular atom positions in (111) plane. Fig. 6 d shows the fragment of diamond-type structure elucidating the location of the positions over depth: the

Fig.5. Fragment of PS (111) at different stages of Si epitaxy (P=0.18, T=1000 K, F=1 bilayer/s).

large circles correspond to the upper surface layer. The positions occupied by atoms are marked in black, those most probable to be occupied - in grey in Figs. 6a,b,c. A white circle inside a black one denotes an atom in the inner bilayer. At first, the metastable nucleus (a chain of atoms or a single atom linked with the structure by two bonds) is formed at the edge of a pore (Fig. 6a). Under certain conditions, depending on temperature and molecular beam density, the metastable nucleus exists long enough to form a bond with a new atom arriving with the surface diffusion flow. The most probable positions to be occupied (grey circles in the Figs. 6a,b,c) are linked with the structure by two bonds at least. At all stages of pendant layer formation these positions appear to be located inside two upper bilayers. Obviously this factor determines the thickness of the pendant layer growing by the perimeter over pore. The analogous series of enlarged fragments near a pore obtained during the computational experiment showed close resemblance with those presented at Figs. 6. The

similar double-linked atomic configurations play the role of metastable nuclei in the simulation process. However, the "coast line" at the edge of the simulated pores is more jagged in comparison with those in Figs. 6.
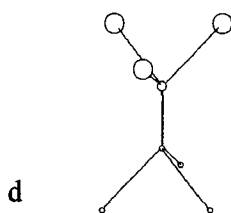
The film growth kinetics and changes in overgrown pore morphology on atomic scale were studied. We have introduced the effective deposited layer thickness, w, which is the amount of Si deposited for pores to be overgrown. The $1/w$ value characterizes the effectiveness of overgrowth.
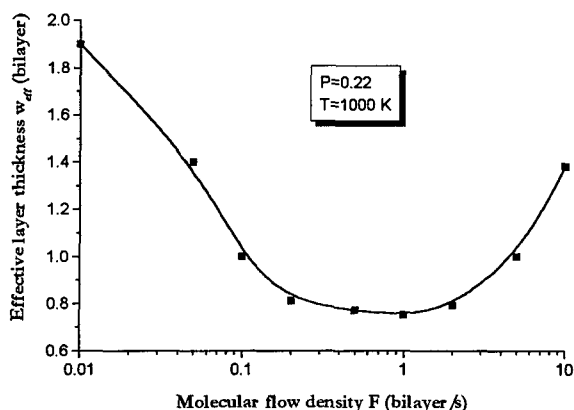
Fig.6. Formation of a pendant layer. Occupied positions are marked in black, those most probable to be occupied next are marked in grey. Figs. a-c illustrate the step-by-step occupation of regular positions inside a pore; d – fragment of diamond type structure elucidating the location of the positions over depth: large circles correspond to the topmost surface layer.

The w vs F is shown in Fig. 7. The porosity is 0.22. In the range of high flow densities (F>2 bilayer/s) w increases while F increases. The explanation is as follows. Under high F the islands nucleate before the pores are overgrown. The higher F leads to a dense distribution of islands between pores. The presence of islands decreases the effectiveness of the overgrowth process since adatoms, which are captured by islands,

Fig. 7. The effective thickness of layer deposited *vs* flow density ($P=0.22$, $T=1000$ K).

cannot form the pendant layer. In the range of moderate flow densities (0.2 bilayer/s<F<1 bilayer/s) w does not depend upon F. Under this condition, the rate of all processes is proportional to F. Under low flow densities (F<0.1 bilayer/s) w increases while F decreases. This effect can be interpreted in terms of the detailed mechanism of pendant layer formation described above. Under low flow density the probability of the transition of the nucleus from a metastable to a stable state decreases, and most of adatoms migrate inside the porous layer. This decreases the effectiveness of overgrowth.

The atomic force microscopy data [19] give an evidence that the surface between pores is rough (with an average relief height ~0.1-0.2 nm). The initial smooth 3D grid ($160\times160\times16$, $P=0.14$) was exposed to an artificial roughening procedure, during which the surface atoms one by one were randomly removed from the grid. The meshes obtained at various intervals were used as the initial substrates in simulation of epitaxy. For numerical characterization of porous layer surface morphology the roughness function, S [12], was calculated and defined as the relative number of atoms situated in the vertical sections of surface.
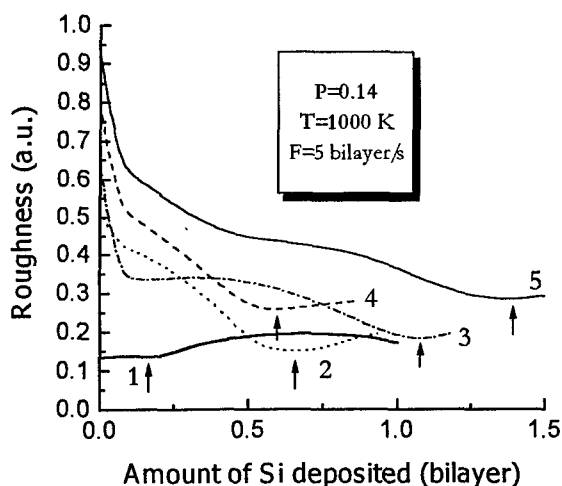

Fig. 8. The dependence of surface roughness upon the amount of Si deposited for various initial surface morphologies ($P=0.14$, $T=1000$ K, $F=5$ bilayer/s).

The dependence of roughness upon the amount of Si deposited is shown in Fig.8 for various initial surface morpholo-

gies (curves 2-5). For comparison, curve 1 is plotted corresponding to the initial surface which is smooth between pores. At the initial stage, curves 2-5 have a sharply descending section, illustrating the effect of polishing. This effect arises due to the intensive capture of adatoms in micropores. The next stage of growth is defined by the competition between the formation of a pendant layer and the growth of islands between pores. Arrows show the points in the curves which correspond to the overgrowth of pores. The interesting result is that w increases non-monotonously with the initial roughness S. The brief explanation of this is as follows. Roughening changes the ratio between the surface areas occupied by the upper and the lower monolayers compiling the (111) bilayer. This leads to a critical change in the effectiveness of the nucleation of islands and accounts for the non-monotonous dependence of w upon initial S. The dependence is not periodical because the removal of monolayers is coupled with the increase in surface roughness.

4. Conclusion

The present model provides a more accurate description of PS formation by electrochemical etching in HF. The simulated structures exhibit close resemblance to those obtained in experiment. The 3D meshes, corresponding qualitatively to nanoporous Si structures, are taken for simulation of Silicon-on-Porous Silicon Epitaxy. The simulation is carried out on the basis of the Gilmer model extended for the case of a relief surface. The possible mechanism of overgrowth of the porous layer is proposed via the pendant layer formation. In terms of this mechanism the dependence of growth kinetics upon the porosity, molecular flow density and initial surface roughness are interpreted.

References

1. Canham L.T. (1990) Silicon quantum wire array fabrication by electrochemical and chemical dissolution of wafers, *Appl. Phys. Lett.* **57**, 1046-1048.
2. Foll H. (1991) Properties of silicon-electrolyte junctions and their application to silicon characterization, *Appl. Phys.* **A53**, 8-19.
3. Shengurov V.G., Shabanov V.N., Gudkov N.V., Tkatch B.Ya. (1993) Epitaxial silicon films formed on the porous silicon surface, *Microelectronics* **222**, 19-23.
4. Yakimov A.I., Stepina N.P., and A.V.Dvurechenskii (1998) Stretched-exponential conductivity relaxation and 1/f noise on fractal networks of porous amorphous silicon, *Phys. Low-Dim. Struct.* **5/6**, 111-130.
5. Smith R.L., Chung S.-H., and Collins S.D. (1988) A theoretical model of the formation morphologies of porous silicon, *J. Electron. Mater.* **17**, 533-547.

6. He J., Huang Y.P., Kwor R. (1995) A modified computer-model for the formation of porous silicon, *Thin Solid Films* **265**, 96-100.

7. Aleksandrov L.N. and Novikov P.L. (1997) Simulation of the formation of porous silicon structures, *JETP Letters* **65**, 714-719.

8. Aleksandrov L.N. and Novikov P.L. (1998) Morphology of porous silicon structures formed by anodization of heavily and lightly doped silicon, *Thin solid films* **330**, 102-107.

9. Aleksandrov L.N. and Novikov P.L. (1996), Kinetics of phase transitions in porous silicon, *phys. stat. sol. (a)* **158**, 419-426.

10. Collins R.T., Fauchet P.M., Tischler M.A. (1997) Porous silicon - from luminescence to LEDs, *Physics Today* **50**, 24-31.

11 . Novikov P.L., Aleksandrov L.N., Dvurechenskii A.V, and Zinovyev V.A.(1999) Modelling of initial stage silicon epitaxy on porous silicon (111) Surface, *Phys. Low-Dim. Struct.* **1/2**, 179-188.

12. Vvedensky D.D.and Clarke Sh. (1990) Recovery kinetics during interrupted epitaxial growth, *Surf. Sci.* **225**, 373-389.

13. Smith R.L.and Collins S.D. (1992) Porous silicon formation mechanisms, *J. Appl. Phys.* **71**, R1-R22.

14. Sasaki Y.and Kitahara M. (1994), Micro-Raman spectroscopy of nanoporous silicon, *J. Appl. Phys.* **76** , 4344-4346.

15. Lehmann V., Hofmann F., Muller F., Cruming U. (1995) Resistivity of porous silicon - a surface effect, *Thin Solid Films* **255**, 20-22.

16. Lehmann V., Hönlein W., Reisinger H., Spitzer A., Wendt H., and Willer J. (1996) A novel capacitor technology based on porous silicon, *Thin Solid Films* **276**, 138-142.

17. Karanovich A.A., Romanov S.I., Kirienko V.V., Myasnikov A.M., and Obodnikov V.I. (1995) A secondary ion mass spectrometry study of p[+] porous silicon, *J. Phys. D-Appl. Phys.* **28**, 2345-2348.

18. Goudeneau P., Naudon A., Bomchil G., and Herino R. (1989) X-ray small-angle scattering analysis of porous silicon layers, *J. Appl. Phys.* **63**, 86-88.

19. Happo N, Fujiwara M., and Horii K. (1998) Atomic-force microscopy study of self-affine fractal roughness of porous silicon surfaces, *Jap. J. Appl. Phys. P1* **37** (1998) 3951-3953.